Acta Crystallographica Section B
Structural Science
ISSN 0108-7681

Octahedral tilting in cation-ordered Jahn–Teller distorted perovskites – a group-theoretical analysis

Christopher J. Howard[a,b] and Michael A. Carpenter[a]*

[a]Department of Earth Sciences, University of Cambridge, Downing Street, Cambridge CB2 3EQ, England, and [b]School of Engineering, University of Newcastle, NSW 2308, Australia

Correspondence e-mail: mc43@esc.cam.ac.uk

Received 10 September 2009
Accepted 12 November 2009

Computer-based group-theoretical methods are used to enumerate structures arising in $A_2BB'X_6$ perovskites, with either rock-salt or checkerboard ordering of the B and B' cations, under the additional assumption that one of these two cations is Jahn–Teller active and thereby induces a distortion of the BX_6 (or $B'X_6$) octahedron. The requirement to match the pattern of Jahn–Teller distortions to the cation ordering implies that the corresponding irreducible representations should be associated with the same point in the Brillouin zone. Effects of BX_6 (and $B'X_6$) octahedral tilting are included in the usual way. Finally, an analysis is presented of more complex models of ordering and distortion as might lead to the doubling of the long axis of the common *Pnma* perovskite, observed in systems such as $Pr_{1-x}Ca_xMnO_3$ ($x \simeq 0.5$). The structural hierarchies derived in this work should prove useful in interpreting experimental results.

1. Introduction

The recent trend in perovskite research has been toward increasingly complex structures and perhaps more exotic applications. At this level, much of the interest is in multiple instabilities and their consequences, while multiferroic properties (Eerenstein *et al.*, 2006; Cheong & Mostovoy, 2007) may be of particular importance. A major driver of this research, in recent times, has been the interest in colossal magnetoresistance (a large change in resistance upon application of magnetic field) that occurs in perovskites based on lanthanum manganite (Chahara *et al.*, 1993; von Helmholt *et al.*, 1993; Jin *et al.*, 1994; Millis, 1998; Chatterji, 2004).

Among the diverse distortions that are found in perovskites, the Jahn–Teller (JT) distortion has particular significance in that it provides a strong link between electronic configuration (*e.g.* orbital ordering) and crystal structure. This link provides the means to study orbital ordering, which is not often directly observable (Lufaso & Woodward, 2004), as well as the means to influence properties that depend on the electronic state. Jahn–Teller distortions in ABX_3 perovskites, and their coupling with the tilting of corner-linked BX_6 octahedra, have been reviewed by Lufaso & Woodward (2004), and the present authors have given a more formal treatment of the symmetries that can arise (Carpenter & Howard, 2009). Perovskites ABX_3, in which the B-site ion is JT active, encompass many structures of interest, including *inter alia* the structure of $LaMnO_3$ (Mn^{3+} being a JT ion) at room temperature (Rodríguez-Carvajal *et al.*, 1998). The current interests, however, extend well beyond those compounds in which every B site is occupied by the same JT-active ionic species. A specific possibility is that half the B sites are occupied by JT-active ions, and half by non-JT ions – the two species of ions

Table 1
The irreps pertaining to perovskites with checkerboard and rock-salt patterns of *B*-site cation ordering, along with those for matched JT distortions, and for octahedral tilting. Entries for checkerboard ordering include order parameters appropriate to ordering on the (001) plane.

Ordering	Cation ordering	JT distortion matched to cation ordering	In-phase octahedral tilting	Out-of-phase octahedral tilting
Checkerboard	M_1^+ (a,0,0)	M_2^+ (b,0,0)	M_3^+	R_4^+
Rock-salt	R_1^+	R_3^+	M_3^+	R_4^+

may or may not be ordered on the *B* site. In their discussion of cation ordering, octahedral tilting and cooperative JT distortion in systems of this nature, Lufaso & Woodward (2004) have examined instances involving rock-salt ordering of the JT/non-JT ions (Ba_2CuWO_6), layered ordering of these two ions (La_2CuSnO_6), checkerboard ordering of different species of manganese ions ($NdSrMn_2O_6$), along with several examples in which the ions are not ordered at all (A_2MnMO_6, A = Ca or Sr, M = Ru, Sb, Ta or Nb). In the field of 'half-doped' manganites, replacement of the trivalent La by a divalent ion such as Ca or Sr leads, at least in principle, to a corresponding replacement of JT-active Mn^{3+} ions by non-JT Mn^{4+}. Although the *B* sites may still all contain Mn, this is no longer uniformly of type Mn^{3+}.

The main purpose in this paper is to extend our own previous group-theoretical treatment combining cooperative Jahn–Teller distortions with octahedral tilting in ABX_3 perovskites (Carpenter & Howard, 2009), to ordered arrangements of stoichiometry $A_2BB'X_6$ in which B and B' represent JT-active and non-JT ions. The analysis (outlined in §2) is applied to rock-salt ordering on the *B* sites, associated with the *R* point of the Brillouin zone (of the cubic parent), and to checkerboard ordering, associated with the *M* point of the same zone. Both these kinds of ordering are characterized by alternating (in checkerboard pattern) B and B' cations within the (001) planes – checkerboard ordering (detailed in §3) refers here to a stack of such planes all similarly aligned, whereas rock-salt ordering (§4) is distinguished by the fact that the B' cation in one plane lies over the B cation in the next. The so-called checkerboard ordering reported in manganites is, however, somewhat more complex, as evidenced by the larger unit cells reported for the structures that are observed. In fact, these structures implicate distortions on the Σ line of symmetry. Accordingly, the paper concludes (§5) with an analysis of three models for these more complex distortions in manganites (all associated with the Σ line), listing in particular the results obtained from combining octahedral tilting with the different distortions proposed. In every case we record details of the structures arising, and the hierarchical relationships between them. Such schemes should prove useful in the interpretation of the experimental results.

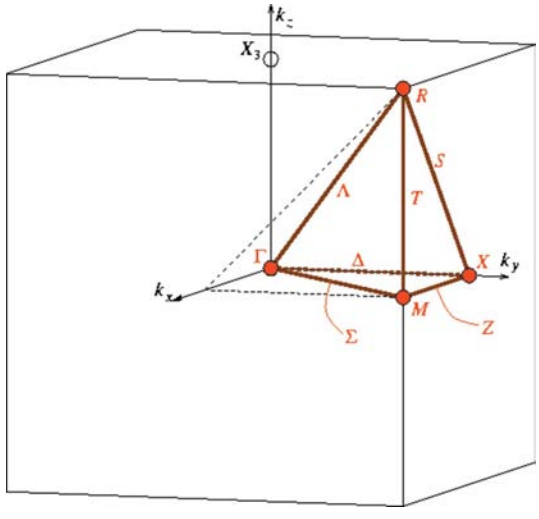

Figure 1
The first Brillouin zone (from the Bilbao Crystallographic Server) corresponding to the primitive cubic lattice, showing points and lines of symmetry. The *M* point ($\boldsymbol{k}$ = $\frac{1}{2},\frac{1}{2}$,0), the *R* point ($\boldsymbol{k}$ = $\frac{1}{2},\frac{1}{2},\frac{1}{2}$), and the Σ ($k$ = ξ,ξ,0) line of symmetry are of particular interest in this work.

2. Group theoretical analysis

The starting structure is the ideal ABX_3 perovskite, cubic in space group $Pm\bar{3}m$. The octahedrally coordinated *B* cation is taken to be at the origin.[1] We consider various possible distortions of this structure and examine the effect of these distortions acting separately or in combination. These different distortions are associated with irreducible representations (irreps) of the parent space-group symmetry. The irreps associated with different distortions of interest have been identified in previous work (Howard & Stokes, 1998, 2005; Carpenter & Howard, 2009). The ubiquitous tilting of the BX_6 octahedra as practically rigid corner-linked units has been analysed in earlier work (Howard & Stokes, 1998). If the sense of tilting in every layer is the same ('in-phase' tilting) this tilting is associated with irrep M_3^+ at the *M* point of the Brillouin zone (Fig. 1), whereas if the sense of this tilting alternates ('out-of-phase' tilting) the distortion is associated with the *R* point and the irrep R_4^+. Carpenter & Howard (2009) considered Jahn–Teller (JT) distortions associated with irreps Γ_3^+, M_2^+, R_3^+ at the Γ, *M* and *R* points, and enumerated the structures resulting from the combination of these distortions with M_3^+ and R_4^+ octahedral tilting. As indicated earlier, the aim in the first part of this paper (§§3 and 4) is to examine the combination of cation ordering on the *B* site, in what are then $A_2BB'X_6$ perovskites, with JT distortions around just one of these cations, say *B*, and octahedral tilting. Rock-salt ordering on the *B* sites is associated with irrep R_1^+ (Howard *et al.*, 2003), and checkerboard ordering on these sites is associated with the *M* point in the Brillouin zone, specifically with irrep M_1^+.

Although cation ordering on the *B* site is associated with specific irreps mentioned above, the general pattern of that

[1] The ideal perovskite could also be set with the *A* cation at the origin, leading to some notational differences in the group-theoretical analysis. Specifically, the distortions to be considered are represented by different irreps.

ordering is determined by the pertinent point in the Brillouin zone. If the JT distortions are to be attached to the B cations, but not to B', then the JT distortions must conform to the same pattern. This means they must be associated with the same point in the Brillouin zone. This is an important principle in the context of the present work. It will imply that the only JT distortion that can combine with checkerboard ordering (M_1^+) is that associated with M_2^+, and the only JT distortion combining with rock-salt ordering (R_1^+) is that associated with R_3^+. There are further implications in the case of checkerboard ordering. Irreps M_1^+ and M_2^+ are both three-dimensional, and the three components of the order parameter correspond to $\boldsymbol{k} = \frac{1}{2},\frac{1}{2},0$, $\boldsymbol{k} = 0,\frac{1}{2},\frac{1}{2}$ and $\boldsymbol{k} = \frac{1}{2},0,\frac{1}{2}$, respectively. Checkerboard ordering on (001) planes rather than (100) or (010) planes is obtained by selecting $\boldsymbol{k} = \frac{1}{2},\frac{1}{2},0$, that is by setting only the first component of the order parameter for M_1^+ non-zero. Pattern matching will be achieved only by selecting $\boldsymbol{k} = \frac{1}{2},\frac{1}{2},0$ for M_2^+, that is by setting the order parameter for this irrep in the same way.[2]

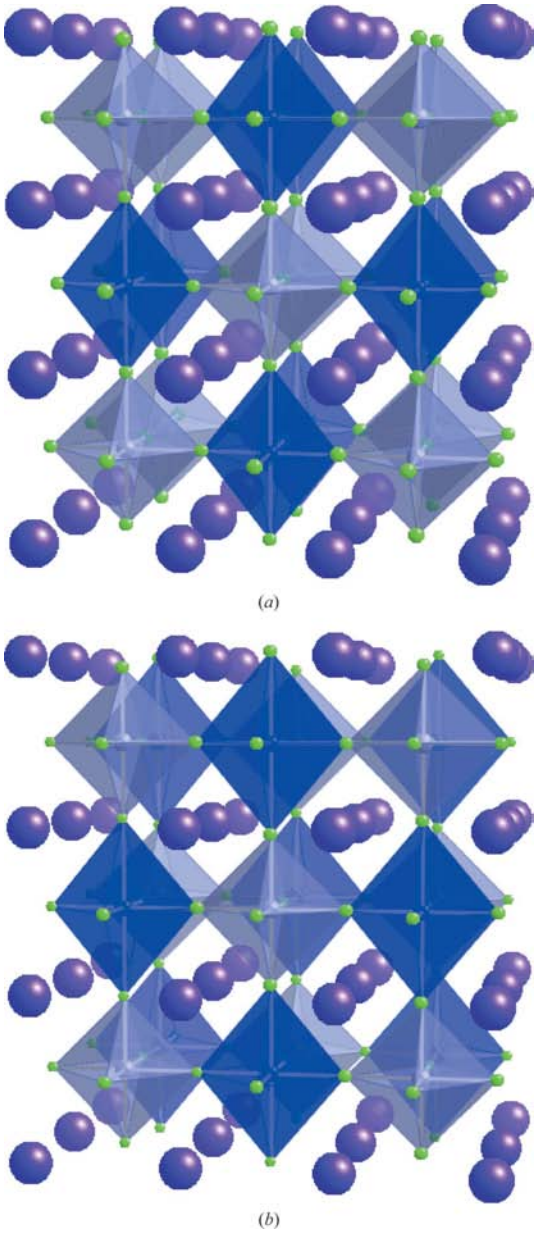

Figure 2
Polyhedral representations of the structures obtained for $A_2BB'X_6$ perovskites with (*a*) checkerboard ordering and (*b*) rock-salt ordering of JT and non-JT cations on the perovskite B site. The JT-active B cation and the JT distorted BX_6 octahedron are shown in blue, while the B' cation and the more regular $B'X_6$ octahedron are shown blue–grey. In checkerboard ordering, the B and B' cations in one layer lie above identical ions in the next, these cations thus forming chains perpendicular to the layers shown, whereas rock-salt ordering has the B and B' cations in one layer lying respectively over the B' and B of the next. This figure was prepared using *CrystalMaker*® (CrystalMaker Software Ltd, 2009).

The different irreps associated with checkerboard and rock-salt ordering of JT and non-JT cations on the B site, with appropriately matching JT distortions, and with both in-phase and out-of-phase octahedral tilting, are collected and presented in Table 1.

There is one further point that merits comment. The effect of irreps M_2^+ and R_3^+, as depicted in Fig. 1 of Carpenter & Howard (2009), is to generate JT distortions around every B-site cation, the distorted BX_6 octahedra being all of the same dimensions, but having orientations differing by 90°. In the structures produced by incorporating the appropriate cation ordering M_1^+ or R_1^+, irrep Γ_3^+, carrying tetragonal and orthorhombic strains, is found to be a secondary distortion. The strains associated with this irrep act to enhance the distortion of octahedra in one orientation while diminishing the distortion of octahedra in the other. It is through this mechanism that we achieve structures, as depicted here in Fig. 2, in which the BX_6 octahedra show significant distortion while the octahedron around $B'X_6$ octahedra are essentially regular.

We acknowledge that the computer-assisted group-theoretical analysis presented herein has been heavily dependent on the computer program *ISOTROPY* and related software (Stokes *et al.*, 2007). First, *ISOTROPY* or *ISODISPLACE* (Campbell *et al.*, 2006) has been used to find the irreps associated with distortions of interest (*e.g.* to find that M_1^+ should be associated with checkerboard ordering of cations). Next, *ISOTROPY* is used to enumerate structures resulting from the different distortions, as represented by irreps, acting separately or in combination. The output lists order parameters for the different structures, and from these order parameters group–subgroup relationships can be found. *ISOTROPY* can be used once more to check the group–subgroup pairs to examine whether, in Landau theory, the corresponding phase transition is allowed to be continuous. (Transitions between structures not so related cannot be continuous.) The approach is described in greater detail in earlier papers, most especially in the Howard & Stokes (2005) review.[3]

[2] No such selection is necessary for rock-salt ordering since two-dimensional checkerboard ordering is found on (001), (100) and (010) planes.
[3] It is stated in this article that 'if the subspace spanned by a particular order parameter has a higher dimension than that spanned by another order parameter, but includes the latter subspace, the isotropy subgroup associated with the second order parameter is a subgroup of that associated with the first order parameter'. In this statement, 'first' and 'second' should be interchanged.

Table 2
Space groups, order-parameter components, tilt systems and unit-cell relationships for simple checkerboard ordering of JT and non-JT ions B and B' in $A_2BB'X_6$ perovskites.

The lattice vectors and origins are given for conventional settings of the space groups and relate to the cell of the ideal cubic perovskite ABX_3 in space group $Pm\bar{3}m$. Irrep M_1^+ with order parameter (a,0,0) specifies the B-site cation ordering, and irrep M_2^+ with order parameter (b,0,0), a matching pattern of JT distortions. The order-parameter components for M_3^+ and R_4^+ correspond respectively to in-phase or out-of-phase octahedral tilting, around axes parallel to the Z, X and Y axes of the starting structure.

Space group	M_1^+	M_2^+	M_3^+	R_4^+	Tilt system	Lattice vectors	Origin
65 *Cmmm*	(*a*,0,0)	(*b*,0,0)	(0,0,0)	(0,0,0)	$a^0b^0c^0$	(2,0,0)(0,2,0)(0,0,1)	(0,0,0)
10 *P2/m*	(*a*,0,0)	(*b*,0,0)	(*c*,0,0)	(0,0,0)	$a^0b^0c^+$	($\bar{1}$,1,0)(0,0,1)(1,1,0)	(0,0,0)
74 *Imma*	(*a*,0,0)	(*b*,0,0)	(0,0,*c*)	(0,0,0)	$a^0b^+c^0$	(0,2,0)(0,0,2)(2,0,0)	(0,0,0)
12 *C2/m*	(*a*,0,0)	(*b*,0,0)	(*c*,*d*,*e*)	(0,0,0)	$a^+b^+c^+$	(2,$\bar{2}$,0)(0,0,2)(0,$\bar{2}$,0)	($\frac{1}{2},\frac{1}{2},\frac{1}{2}$)
66 *Cccm*	(*a*,0,0)	(*b*,0,0)	(0,0,0)	(*c*,0,0)	$a^0b^0c^-$	(2,0,0)(0,2,0)(0,0,2)	(0,0,0)
63 *Cmcm*	(*a*,0,0)	(*b*,0,0)	(0,0,0)	(0,0,*c*)	$a^0b^-c^0$	(0,2,0)($\bar{2}$,0,0)(0,0,2)	(0,0,0)
15 *C2/c*	(*a*,0,0)	(*b*,0,0)	(0,0,0)	(*c*,*d*,0)	$a^-b^0c^-$	(2,0,0)(0,2,0)(0,0,2)	(0,0,0)
2 $P\bar{1}$	(*a*,0,0)	(*b*,0,0)	(0,0,0)	(*c*,*d*,*e*)	$a^-b^-c^-$	(0,0,2)(1,1,0)($\bar{1}$,1,0)	(0,0,0)
52 *Pnna*	(*a*,0,0)	(*b*,0,0)	(0,0,*c*)	(*d*,0,0)	$a^0b^+c^-$	(0,0,2)(0,2,0)($\bar{2}$,0,0)	(0,0,0)
62 *Pnma*	(*a*,0,0)	(*b*,0,0)	(0,0,*c*)	(0,*d*,0)	$a^-b^+c^0$	(0,2,0)(0,0,2)(2,0,0)	(0,0,0)
11 $P2_1/m$	(*a*,0,0)	(*b*,0,0)	(*c*,0,0)	(0,*d*,*e*)	$a^-b^-c^+$	($\bar{1}$,1,0)(0,0,2)(1,1,0)	(0,0,0)
13 *P2/c*	(*a*,0,0)	(*b*,0,0)	(*c*,*d*,*e*)	(*f*,0,0)	$a^+b^+c^-$	($\bar{2}$,0,0)(0,0,2)(2,2,0)	(0,0,0)

3. Checkerboard ordering

By checkerboard ordering we mean the alternation of B and B' cations within each layer, and the stacking of the layers so that each is identical to the one below. This is sometimes called 'chain' ordering since the B and B' ions run in chains normal to the plane of the checkerboard. The irrep is M_1^+, at $\boldsymbol{k} = \frac{1}{2},\frac{1}{2},0$, and the structure arising in an $A_2BB'X_6$ perovskite with just checkerboard ordering has space-group symmetry $P4/mmm$ on an $a_p2^{1/2} \times a_p2^{1/2} \times a_p$ cell, a_p representing the cell edge of the $Pm\bar{3}m$ parent.

This is not yet the checkerboard-type model proposed for half-doped manganites (see for example Subías *et al.*, 2006). As we shall see (§5), this model implies checkerboard ordering of the Mn cations, but incorporates additional distortions around the JT-active ions leading to a larger unit cell.

The requirement for pattern-matching means that we need consider only those JT distortions corresponding to the M point, paying particular attention to the anion (X) displacements associated with the different irreps. We find as before (Carpenter & Howard, 2009) a JT distortion associated with irrep M_2^+. There are other irreps at the M point giving rise to anion displacements. It is not surprising to find among these, M_1^+, corresponding to a checkerboard arrangement of larger and smaller BX_6 ($B'X_6$) octahedra on the B and B' ions. Octahedral tilting can also be recognized (M_3^+). Although there are still others, such as shearing of the octahedron in its equatorial plane (M_4^+), none of these could be construed as distortions of JT type.

Combining the distortions associated with checkerboard cation ordering in $A_2BB'X_6$ (irrep M_1^+) with a JT distortion around one of the cations, say B, (irrep M_2^+)[4] leads to a structure (the first entry in Table 2) in space group *Cmmm* on a $2a_p \times 2a_p \times a_p$ cell. This structure is illustrated in Fig. 2(*a*), which is an adaptation to the lower symmetry of Fig. 1(*a*) from Carpenter & Howard (2009).

In order to examine the effects on this structure of octahedral tilting, we use *ISOTROPY* to enumerate the structures obtained by combining with $M_1^+ + M_2^+$ first M_3^+, then R_4^+, and finally $M_3^+ + R_4^+$. The results from this analysis are indicated in Fig. 3 and shown in detail in Table 2. Table 2 lists the space groups for different structures along with the lattice vectors and origin referred to the lattice vectors and origin of the $Pm\bar{3}m$ starting perovskite, the order parameters relating to the different irreps involved, and the tilt system in Glazer's (1972) notation. In fact we do not show all the structures listed by *ISOTROPY*. For example, *ISOTROPY* lists structures with various M_1^+ and M_2^+ order parameters, but we select just those with only the first component non-zero in order to obtain the checkerboard pattern of interest. In addition, we have followed the usual practice of removing structures showing in-phase (M_3^+) and out-of-phase (R_4^+) tilts around the same axis (that is, the corresponding order parameters both have a particular component different from zero), although we have relaxed this condition for the last entry (space group *P2/c*), since this gives a tilt system not otherwise accessible. The structures detailed in Table 2 are arranged in Fig. 3 to show the group–subgroup relationships. These relationships are determined in the usual manner (Howard & Stokes, 2005) from an inspection of the order parameters. By selecting only those structures with order parameters (a,0,0) and (b,0,0) for M_1^+

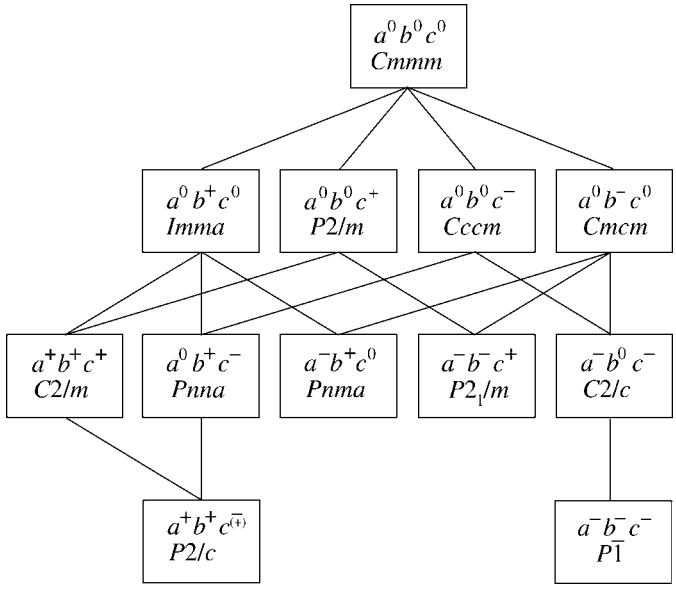

Figure 3
A schematic diagram showing the group–subgroup relationships among the structures formed in double perovskites $A_2BB'X_6$ with a checkerboard ordering pattern of JT-active B cations and non-active B' cations; by this we mean a checkerboard alternation of JT-distorted BX_6 octahedra with nearly regular $B'X_6$ octahedra. The lines connecting structures indicate group–subgroup relationships and all the corresponding transitions are, in Landau theory, allowed to be continuous. Details of the structures are recorded in Table 2.

[4] Taking care that order parameter components in each case are set to select $\boldsymbol{k} = \frac{1}{2},\frac{1}{2},0$.

Table 3
Space groups, order-parameter components, tilt systems and unit-cell relationships for rock-salt ordering of JT and non-JT ions B and B' in $A_2BB'X_6$ perovksites.

The presentation of results is as in Table 2.

Space group	R_1^+	R_3^+	M_3^+	R_4^+	Tilt system	Lattice vectors	Origin
139 *I*4/*mmm*	(*a*)	(*b*,0)	(0,0,0)	(0,0,0)	$a^0a^0c^0$	(1,1,0)($\bar{1}$,1,0)(0,0,2)	(0,0,0)
128 *P*4/*mnc*	(*a*)	(*b*,0)	(*c*,0,0)	(0,0,0)	$a^0a^0c^+$	(1,1,0)($\bar{1}$,1,0)(0,0,2)	(0,0,0)
134 $P4_2/nnm$	(*a*)	(*b*,0)	(0,*c*,*c*)	(0,0,0)	$a^+a^+c^0$	(2,0,0)(0,2,0)(0,0,2)	(0,0,0)
48 *Pnnn*	(*a*)	(*b*,*c*)	(*d*,*e*,*f*)	(0,0,0)	$a^+b^+c^+$	(2,0,0)(0,2,0)(0,0,2)	(0,0,0)
87 *I*4/*m*	(*a*)	(*b*,0)	(0,0,0)	(*c*,0,0)	$a^0a^0c^-$	(1,1,0)($\bar{1}$,1,0)(0,0,2)	(0,0,0)
12 *C*2/*m*	(*a*)	(*b*,0)	(0,0,0)	(0,*c*,*c*)	$a^-a^-c^0$	($\bar{1}$,1,$\bar{2}$)(1,1,0)(1,$\bar{1}$,0)	(0,0,0)
2 $P\bar{1}$	(*a*)	(*b*,*c*)	(0,0,0)	(*d*,*e*,*f*)	$a^-b^-c^-$	(1,0,1),(1,1,0),($\bar{1}$,1,0)	(0,0,0)
15 *C*2/*c*	(*a*)	(*b*,*c*)	(*d*,0,0)	(0,0,*e*)	$a^0b^-c^+$	(2,0,0)(0,2,0)(0,0,2)	($\frac{1}{2}$,$\frac{1}{2}$,0)
86 $P4_2/n$	(*a*)	(*b*,0)	(0,*c*,*c*)	(*d*,0,0)	$a^+a^+c^-$	(2,0,0)(0,2,0)(0,0,2)	(1,0,0)
14 $P2_1/c$	(*a*)	(*b*,0)	(*c*,0,0)	(0,*d*,*d*)	$a^-a^-c^+$	(1,$\bar{1}$,0),(1,1,0)(1,$\bar{1}$,2)	(0,0,0)

and M_2^+, we have set the ordering onto the (001) plane and so made the Z-direction unique. We note, however, that the second and third components of the order parameter corresponding to the X and Y directions can be interchanged. This implies that the structure in *Pnma* with R_4^+ order parameter (0,d,0) shows as a subgroup of that in *Cmcm*, with R_4^+ order parameter (0,0,c), but is not similarly related to the structure in *Cccm*, where this order parameter is (c,0,0). It has been confirmed using *ISOTROPY* that, for every group–subgroup pair found here, the corresponding transition is allowed to be continuous.

4. Rock-salt ordering

Rock-salt ordering of two distinct B-site cations to give perovskites of the stoichiometry $A_2BB'X_6$, and its combination with octahedral tilting, formed the subject of an earlier study (Howard *et al.*, 2003). The irrep associated with such ordering is R_1^+, and the structure which results from just this ordering is cubic in $Fm\bar{3}m$ on a $2a_p \times 2a_p \times 2a_p$ cell. Matching the JT distortions to the cation ordering means we look for irreps at the R point, and we find as before (Carpenter & Howard, 2009) that the relevant irrep is R_3^+. The structure formed by combining B cation ordering with the R_3^+ pattern of JT distortions is, in the absence of tilting, a structure in space group *I*4/*mmm* on a $a_p2^{1/2} \times a_p2^{1/2} \times a_p$ cell. This structure is illustrated in Fig. 2(*b*) (essentially a view down [110]), where it can be discerned that the distorted octahedron in one layer lies directly over the undistorted octahedron in the layer below. In this structure, the octahedral distortion involves the expansion (or contraction) of two $B-X$ bonds and the contraction (or expansion) of the remaining four $B-X$ bonds such that both distorted (BX_6) and undistorted ($B'X_6$) octahedra retain fourfold symmetry – this distortion is commonly labelled Q_3 (Goodenough, 1998, 2004). As will be seen in Table 3, the value for the order parameter for R_3^+ in this situation is (b,0). There is the possibility of an element of distortion of the type labelled Q_2, leading to an orthorhombic distortion and a structure in space group *Fmmm* on a $2a_p \times 2a_p \times 2a_p$ cell, the R_3^+ order parameter for this structure being (b,c). The structure corresponding to the R_3^+ order parameter (0,b), although favoured in JT distorted ABX_3 perovskites (Carpenter & Howard, 2009), is incompatible with the rock-salt arrangement R_1^+ of two different cations B and B'.

We use *ISOTROPY* to examine the effects on the *I*4/*mmm* structure (incorporating both R_1^+ cation ordering and R_3^+ JT distortions) by combining these distortions with octahedral tilting distortions M_3^+ and R_4^+. The results are detailed in Table 3. Once again we show only a selection of the structures listed by *ISOTROPY*. We exclude structures with two non-zero components of R_3^+ (b,c) for tilt systems that can be obtained with the R_3^+ order parameter (b,0) as well as those showing M_3^+ and R_4^+ tilts around the same axis. The structures listed in Table 3 are arranged in Fig. 4 to show group–subgroup relationships, and it has been confirmed that for every group–subgroup relationship the corresponding phase transition is permitted to be continuous. A comparison with the results obtained previously for rock-salt ordered perovskites (Howard *et al.*, 2003) shows that the effect of the R_3^+ JT distortion is to lower the space-group symmetry of the untilted structure from $Fm\bar{3}m$ to *I*4/*mmm* and to remove the two structures with threefold symmetry axes from the scheme. Further analysis shows that the transition $Fm\bar{3}m$ to *I*4/*mmm* induced by JT distortion of the rock-salt ordered cubic perovskite is necessarily first order.

The untilted but JT distorted structure in *I*4/*mmm* has been found in Sr_2CuWO_6 above 873 K by Gateshki *et al.* (2003), this identification being supported by the observation at around 1173 K of the first-order transition to the undistorted rock-salt ordered structure in $Fm\bar{3}m$. The structure at room temperature is taken to be tilt system $a^0a^0c^-$ in space group *I*4/*m*, and consistent with this assignment the transition at around 873 K is judged to be continuous. With regard to the tilted structures, such as this one in *I*4/*m*, there is nothing in the space-group symmetry to distinguish a JT distorted structure from one not

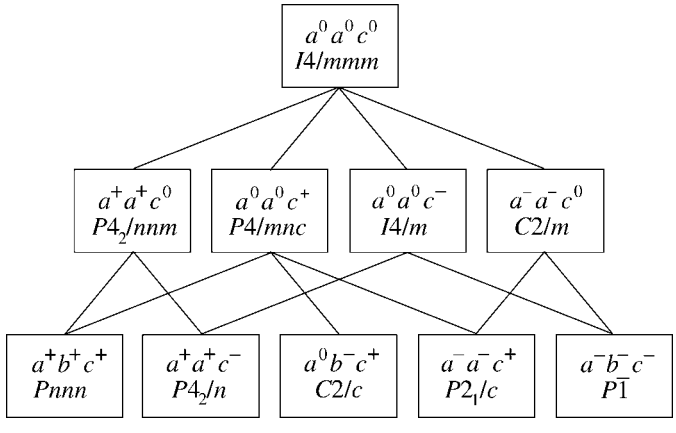

Figure 4
A schematic diagram showing, in a manner similar to Fig. 3, the group–subgroup relationships among the structures formed in double perovskites $A_2BB'X_6$ with a rock-salt ordering of JT-active B cations (implying JT-distorted BX_6 octahedra) and non-active B' cations. Details of the structures are to be found in Table 3.

so distorted, so the presence of JT distortion must be inferred from the dimensions of the two different octahedra. From the published data (Gateshki & Igartua, 2003), we calculate the bond lengths in the CuO_6 octahedron to be 2.300 Å (×2) and 1.962 Å (×4) and the bond lengths in the WO_6 octahedron to be 1.899 Å (×2) and 1.918 Å (×4). The CuO_6 octahedron is clearly elongated, which we take to be a JT distortion, whereas the WO_6 octahedron is close to regular. In their review of cation-ordered JT perovskites, Lufaso & Woodward (2004) reported the general occurrence of this same structure type (tilt system $a^0a^0c^-$, space group $I4/m$) in the series A_2CuMO_6, with A = Ba or Sr and M = W or Te. Subsequently, Sr_2CuOsO_6 was found to adopt the same structure (Lufaso *et al.*, 2008). There are also reports on the perovskite Sr_2MnSbO_6 (Cheah *et al.*, 2006; Ivanov *et al.*, 2009) that suggest this is an incompletely ordered but nevertheless JT distorted perovskite with the same tilt and space-group symmetry, that transforms directly and continuously at 750 K to the cubic perovskite in $Fm\bar{3}m$. Finally we note that Mclaughlin (2008) has claimed a JT distortion in Ba_2SmMoO_6 below 130 K, along with a lowering of symmetry from $I4/m$ to $P\bar{1}$.

5. More complex ordering

More complex patterns of ordering have been encountered in studies of half-doped manganites, $R_{1/2}A_{1/2}MnO_3$, where R is a trivalent rare-earth ion, A is a divalent alkaline-earth ion, and accordingly Mn has an average valence of 3.5. It was recognized many years ago (Wollan & Koehler, 1955; Goodenough, 1955) that the low-temperature magnetic structures of such compounds, specifically $La_{1-x}Ca_xMnO_3$, could be complex, but their propensity to display colossal magnetoresistance, responsible for the resurgence of interest in these compounds, was discovered somewhat more recently (Jin *et al.*, 1994). The focus here will be on the crystal structures.

At room temperature, these half-doped manganite perovskites adopt the common structures of ABX_3 perovskites with octahedral tilting only (Howard & Stokes. 1998). The structures appear to be determined primarily by the sizes of the A-site cations, with the smaller cations giving rise to more elaborate patterns of tilting, that is to say tilt systems characterized by a greater number of independent tilt angles. For example, $La_{1/2}Ba_{1/2}MnO_3$ seems to be cubic in $Pm\bar{3}m$ (no tilting; Ju *et al.*, 2000), $La_{1/2}Sr_{1/2}MnO_3$ and $Pr_{1/2}Sr_{1/2}MnO_3$ adopt the $I4/mcm$ structure (tilt system $a^0a^0c^-$; Sundaresan *et al.*, 1998; Argyriou *et al.*, 1996; Damay *et al.*, 1998), $Nd_{1/2}Sr_{1/2}MnO_3$ crystallizes in the space group $Imma$ ($a^-a^-c^0$; Caignaert *et al.*, 1996; Woodward *et al.*, 1999), whereas at room temperature $La_{1/2}Ca_{1/2}MnO_3$ and $Pr_{1/2}Ca_{1/2}MnO_3$ form structures in $Pnma$ ($a^-a^-c^+$; Radaelli *et al.*, 1997; Jirák *et al.*, 2000; Daoud-Aladine *et al.*, 2002). None of these structures provide more than one distinct B site (here Mn), so charge ordering within them is precluded.

Complex patterns, presumed due to charge and/or orbital (JT) ordering, are found in certain of the above compounds at lower temperatures. The structures observed are characterized by a larger unit cell, of approximate dimensions $2(2)^{1/2}a_p \times 2a_p \times 2^{1/2}a_p$, where the additional factor 2 in the first dimension may arise in either commensurate or incommensurate fashion. Nuclear superlattice peaks corresponding to such enlargement seem to have been noted first by Jirák *et al.* (1985) in neutron diffraction patterns from $Pr_{1/2}Ca_{1/2}MnO_3$ at helium temperature. These authors proposed a structure in accordance with the Goodenough (1955) model, incorporating a simple checkerboard ordering of Mn^{3+} and Mn^{4+} ions together with a longer-range pattern of JT distortions centred on the Mn^{3+} ions (see Fig. 3 in Jirák *et al.*, 1985). Radaelli and co-workers (Radaelli *et al.*, 1995, 1997) carried out a detailed investigation of the low-temperature (20 K) structure of $La_{1/2}Ca_{1/2}MnO_3$, observed superlattice reflections corresponding to a slightly incommensurate version of the doubling, and developed a similar model, with a not quite commensurate pattern of JT distortions on the Mn^{3+} ions. Other half-doped manganites reported to adopt similar charge/orbitally ordered structures include $Tb_{1/2}Ca_{1/2}MnO_3$ (Blasco *et al.*, 1997) and $Nd_{1/2}Sr_{1/2}MnO_3$ (Shimomura *et al.*, 1999; Woodward *et al.*, 1999). A problem with the Goodenough model was encountered, however, when charges estimated from bond-valence sums were 3.42 and 3.88, as against the expected values of 3 and 4 (Jirák *et al.*, 2000). This problem was exacerbated following a careful neutron diffraction single-crystal study of $Pr_{0.60}Ca_{0.40}MnO_3$ (Daoud-Aladine *et al.*, 2002) that implied valences on the two distinct Mn ions of 3.50 and 3.53. Accordingly, Daoud-Aladine *et al.* (2002) proposed a different model for the longer-range ordering, involving not Mn^{3+}/Mn^{4+} charge separation but the formation of Mn–Mn dimers in an arrangement giving a similar final cell. This has been variously styled the 'Zener polaron' or 'bond-centred' model. A third model arises from an investigation using both electron diffraction and high-resolution electron microscopy of $Bi_{1/2}Sr_{1/2}MnO_3$, which is ordered at room temperature (Hervieu *et al.*, 2001). In contrast to the checkerboard charge-ordering arrangement, which has Mn^{3+} and Mn^{4+} on alternate (110) planes[5] [where again we have set the ordering pattern onto the (001) planes], this new structure is considered to show two successive (110) planes of Mn^{3+} followed by two successive planes of Mn^{4+}. The ordering in the first of these two models is described as 'striped' and in the second as 'bistriped'. There is as yet no final agreement on which (if any) of the above models provides the most appropriate description of the charge and/or orbitally ordered half-doped manganites (Goff & Attfield, 2004; Loudon *et al.*, 2005; Subías *et al.*, 2006; Wu *et al.*, 2007), nor indeed whether different models may be needed for the different examples. There is, however, a near to general consensus that the unit cell of the ordered superstructure is related to that of the $Pnma$ perovskite (on a $2^{1/2}a_p \times 2a_p \times 2^{1/2}a_p$ cell) by a doubling of the a dimension, at least approximately, to give the final $2(2)^{1/2}a_p \times 2a_p \times 2^{1/2}a_p$ cell.

[5] The indexing in this section references the cubic parent in $Pm\bar{3}m$.

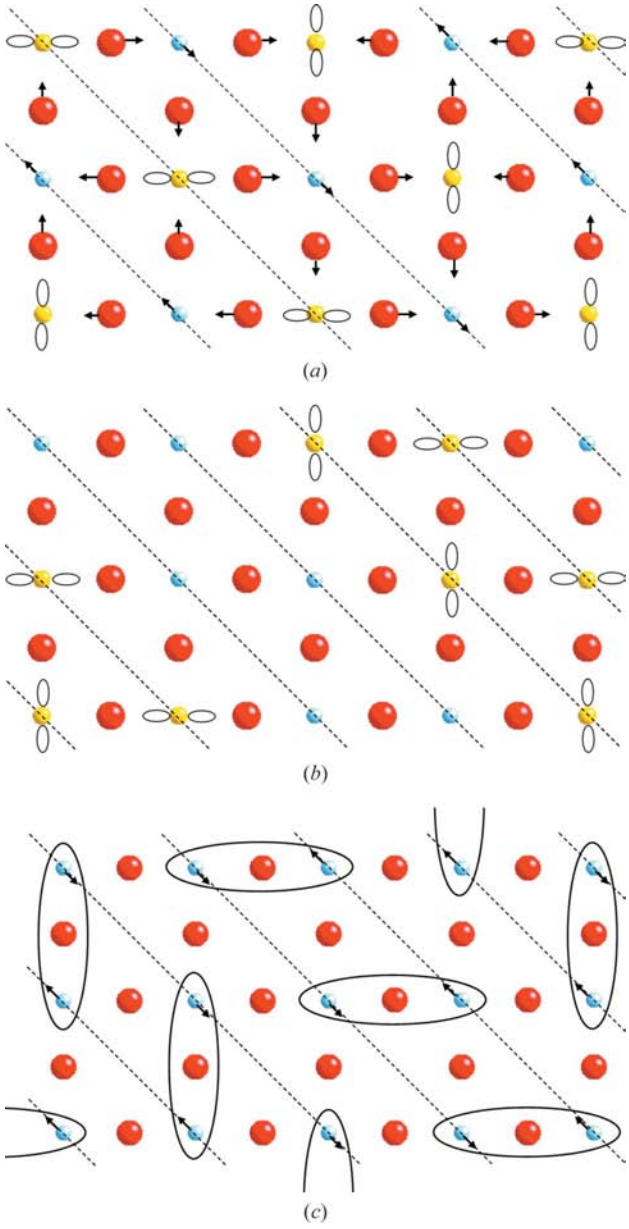

Figure 5
Illustrations of three models proposed for the longer period ordering in half-doped manganites. These show the (001) planes (indexing on the cubic parent cell) containing the manganese ions (smaller spheres) along with oxygen (large spheres). Such planes are reproduced unchanged in the third dimension. The dashed lines show the intersections of (110) planes of manganese ions with these planes [these would be indexed (11) on the two-dimensional representation]. The lobes on some ions represent orbital ordering on what are considered to be Mn^{3+}, and arrows indicate directions of displacements from starting positions in the cubic structure. In the 'striped' or 'checkerboard-type' model shown in (*a*) planes of notionally Mn^{3+} ions, which are not displaced, alternate with planes of notionally Mn^{4+} ions that are expected to be displaced along $[1\bar{1}0]$ and $[\bar{1}10]$, the sense reversing from one Mn^{4+} plane to the next. In the 'bistriped' model shown in (*b*) two planes of Mn^{3+} are followed by two planes of Mn^{4+} and this charge ordering in itself delivers the required periodicity. In the Zener polaron or dimer model shown in (c) there is no necessity for charge separation since the periodicity is developed by displacing manganese ions in two successive (110) planes along [110] and in the next two planes in the reverse sense. The ellipses indicate where the dimers are formed.

The doubling of the cell edge *a* of the *Pnma* perovskite is associated with the *X* point ($\boldsymbol{k} = \frac{1}{2},0,0$ for this structure), which corresponds[6] to a point on the Σ ($\boldsymbol{k} = \xi,\xi,0$) line of symmetry in the Brillouin zone of the parent cubic perovskite in $Pm\bar{3}m$. There are four irreps, Σ_1, Σ_2, Σ_3, Σ_4 associated with points on this line of symmetry, and all are 12-dimensional. The analysis to be presented here is for the commensurate case, $\xi = 1/4$.

In the checkerboard (striped) model, the doubling of the *Pnma* cell of the perovskite is not due to charge ordering (it should be evident from §3 that checkerboard charge ordering will not produce a cell of the required dimension), but rather it is due to orbital ordering and the concomitant JT distortion. The model is illustrated in Fig. 5(*a*), in which Mn^{3+} and Mn^{4+} are thought to occupy alternate (110) planes as for simple checkerboard ordering, but the orientation of the orbitals on Mn^{3+} changes from one Mn^{3+} plane to the next. The JT distortions (indicated) also imply the displacement of Mn^{4+} ions in the directions $[1\bar{1}0]$ and $[\bar{1}10]$, the sense reversing from one of these Mn^{4+} planes to the next. It is found, using *ISOTROPY* or *ISODISPLACE*, that this pattern is obtained from irrep Σ_2 (direction $P1$[7]), and the same irrep (direction) produces displacements of the oxygen ions in accordance with the pattern of JT distortions envisaged here. As recognized in fact by Jirák *et al.* (1985), the structure arising from this distortion has space-group symmetry *Pmma* and a $2(2)^{1/2}a_p \times a_p \times 2^{1/2}a_p$ cell (first entry in Table 4). A complete listing of order parameters using *ISOTROPY* or *COPL* (Stokes & Hatch, 2001) includes (as a secondary) irrep M_1^+ with order parameter (a,0,0). This can be recognized as the checkerboard charge ordering of §3, but the analysis here suggests it may be but a secondary effect. Thus, from a symmetry point of view, experimental evidence pointing to only a small degree of charge separation (Radaelli *et al.*, 1997; Daoud-Aladine *et al.*, 2002) is not a problem, but this does pose a problem from a conceptual point of view because without significant charge separation it is difficult to understand why orbital ordering affects only alternate planes of Mn ions in the manner depicted. The structure with this *Pmma* pattern of distortions together with *Pnma* tilting has space-group symmetry $P2_1/m$.

In the bistriped model, the required periodicity can be achieved simply by supposing that two successive (110) planes are occupied by one species, say Mn^{3+}, and the next two by the other, say Mn^{4+}. Now the only irrep that permits a variation of occupancy on the Wyckoff *a* site of $Pm\bar{3}m$ is Σ_1, and Σ_1 (direction $P2$) yields just this bistripe pattern of occupancy (Fig. 5*b*). The structure arising from these bistripe occupancies $\Sigma_1(P2)$ also has space-group symmetry *Pmma*, but now on a $2^{1/2}a_p \times a_p \times 2(2)^{1/2}a_p$ cell (see also Table 5). Although this structure does not depend on orbital ordering, a possible

[6] This is established by noting that the lattice vectors and origin of the structure in *Pnma* in terms of the lattice vectors and origin of the cubic in $Pm\bar{3}m$ are (110), (002), (1,$\bar{1}$,0) and (0,0,0), then following the standard procedures for transforming reciprocal space coordinates (see for example chapter 5 in Kisi & Howard, 2008).
[7] The order parameters for directions $P1$ and $P2$ of the irreps on the Σ line of symmetry are (0,*a*,0,0,0,0,0,0,0,0,0,0) and (0,*a*,*a*,0,0,0,0,0,0,0,0,0).

Table 4
Space groups, order-parameter components, and unit-cell relationships for the so-called checkerboard ordering in manganites, associated with the irrep Σ_2 ($\boldsymbol{k} = \xi,\xi,0$, $\xi = 1/4$).

The order-parameter components for M_3^+ and R_4^+ correspond respectively, as before, to in-phase or out-of-phase octahedral tilting, around axes parallel to the Z, X and Y axes of the starting structure.

Space group	Σ_2	M_3^+	R_4^+	Lattice vectors	Origin
51 *Pmma*	(0,*a*,0,0,0,0,0,0,0,0,0,0)	(0,0,0)	(0,0,0)	(2,$\bar{2}$,0)(0,0,$\bar{1}$)(1,1,0)	(0,0,0)
10 *P*2/*m*	(0,*a*,0,0,0,0,0,0,0,0,0,0)	(*b*,0,0)	(0,0,0)	(2,$\bar{2}$,0)(0,0,$\bar{1}$)(1,1,0)	(0,0,0)
63 *Cmcm*	(0,*a*,0,0,0,0,0,0,0,0,0,0)	(0,*b*,*b*)	(0,0,0)	(0,0,2)(2,2,0)($\bar{2}$,2,0)	($\frac{1}{2}$,$\frac{1}{2}$,$\frac{1}{2}$)
64 *Cmca*	(0,*a*,0,0,0,0,0,0,0,0,0,0)	(0,*b*,−*b*)	(0,0,0)	(0,0,2)(2,2,0)($\bar{2}$,2,0)	($\frac{1}{2}$,$\frac{1}{2}$,$\frac{1}{2}$)
12 *C*2/*m*	(0,*a*,0,0,0,0,0,0,0,0,0,0)	(*b*,*c*,*d*)	(0,0,0)	(2,2,0)(0,0,2)(2,$\bar{2}$,0)	($\frac{1}{2}$,$\frac{1}{2}$,$\frac{1}{2}$)
53 *Pmna*	(0,*a*,0,0,0,0,0,0,0,0,0,0)	(0,0,0)	(*b*,0,0)	(0,0,2)(1,1,0)($\bar{2}$,2,0)	(0,0,0)
57 *Pbcm*	(0,*a*,0,0,0,0,0,0,0,0,0,0)	(0,0,0)	(0,*b*,*b*)	(1,1,0)($\bar{2}$,2,0)(0,0,2)	(0,0,0)
59 *Pmmn*	(0,*a*,0,0,0,0,0,0,0,0,0,0)	(0,0,0)	(0,*b*,−*b*)	(2,$\bar{2}$,0)(0,0,$\bar{2}$)(1,1,0)	(0,0,0)
14 $P2_1/c$	(0,*a*,0,0,0,0,0,0,0,0,0,0)	(0,0,0)	(*b*,*c*,*c*)	(1,1,0)($\bar{2}$,2,0)(0,0,2)	(0,0,0)
13 *P*2/*c*	(0,*a*,0,0,0,0,0,0,0,0,0,0)	(0,0,0)	(*b*,*c*,−*c*)	(0,0,2)(1,1,0)($\bar{2}$,2,$\bar{2}$)	(0,0,0)
52 *Pnna*	(0,*a*,0,0,0,0,0,0,0,0,0,0)	(0,*b*,*b*)	(*c*,0,0)	(2,2,0)($\bar{2}$,2,0)(0,0,2)	(0,0,0)
60 *Pbcn*	(0,*a*,0,0,0,0,0,0,0,0,0,0)	(0,*b*,−*b*)	(*c*,0,0)	(2,$\bar{2}$,0)(0,0,$\bar{2}$)(2,2,0)	(0,0,0)
11 $P2_1/m$	(0,*a*,0,0,0,0,0,0,0,0,0,0)	(*b*,0,0)	(0,*c*,*d*)	(2,$\bar{2}$,0)(0,0,$\bar{2}$)(1,1,0)	(0,0,0)
2 $P\bar{1}$	(0,*a*,0,0,0,0,0,0,0,0,0,0)	(*b*,0,0)	(*c*,*d*,*e*)	(0,0,2)(1,1,0)($\bar{2}$,2,0)	(0,0,0)

Table 5
Space groups, order-parameter components, and unit-cell relationships for bistripe ordering in manganites, associated with the irrep Σ_1 ($\boldsymbol{k} = \xi,\xi,0$, $\xi = 1/4$).

The presentation of results is as in Table 4.

Space group	Σ_1	M_3^+	R_4^+	Lattice vectors	Origin
51 *Pmma*	(0,*a*,−*a*, 0,0,0,0,0,0,0,0,0)	(0,0,0)	(0,0,0)	(1,1,0)(0,0,1)(2,$\bar{2}$,0)	($\frac{1}{2}$,0,0)
26 $Pmc2_1$	(0,*a*,−*a*, 0,0,0,0,0,0,0,0,0)	(*b*,0,0)	(0,0,0)	(0,0,1)(2,$\bar{2}$,0)(1,1,0)	($\frac{3}{4}$,$\frac{1}{4}$,0)
12 *C*2/*m*	(0,*a*,−*a*, 0,0,0,0,0,0,0,0,0)	(0,*b*,0)	(0,0,0)	(2,2,0)(0,0,2)(2,$\bar{2}$,0)	(0,$\frac{3}{2}$,$\frac{1}{2}$)
35 *Cmm*2	(0,*a*,−*b*, 0,0,0,0,0,0,0,0,0)	(0,*c*,*c*)	(0,0,0)	(0,0,2)(2,2,0)($\bar{2}$,2,0)	(0,0,$\frac{1}{2}$)
8 *Cm*	(0,*a*,−*b*, 0,0,0,0,0,0,0,0,0)	(*c*,*d*,*e*)	(0,0,0)	(2,2,0)(0,0,2)(2,$\bar{2}$,0)	(0,0,$\frac{1}{2}$)
57 *Pbcm*	(0,*a*,−*a*, 0,0,0,0,0,0,0,0,0)	(0,0,0)	(*b*,0,0)	(2,$\bar{2}$,0)(1,1,0)(0,0,2)	($\frac{1}{2}$,0,$\frac{1}{2}$)
51 *Pmma*	(0,*a*,−*a*, 0,0,0,0,0,0,0,0,0)	(0,0,0)	(0,*b*,*b*)	(1,1,0)(0,0,2)(2,$\bar{2}$,0)	($\frac{1}{2}$,0,$\frac{1}{2}$)
53 *Pmna*	(0,*a*,−*a*, 0,0,0,0,0,0,0,0,0)	(0,0,0)	(0,*b*,−*b*)	(0,0,2)(2,$\bar{2}$,0)(1,1,0)	($\frac{1}{2}$,0,$\frac{1}{2}$)
13 *P*2/*c*	(0,*a*,−*a*, 0,0,0,0,0,0,0,0,0)	(0,0,0)	(*b*,*c*,*c*)	(0,0,2)(2,$\bar{2}$,0)(1,1,0)	($\frac{1}{2}$,0,$\frac{1}{2}$)
14 $P2_1/c$	(0,*a*,−*a*, 0,0,0,0,0,0,0,0,0)	(0,0,0)	(*b*,*c*,−*c*)	(2,$\bar{2}$,0)(1,1,0)(0,0,2)	($\frac{1}{2}$,0,$\frac{1}{2}$)
10 *P*2/*m*	(0,*a*,−*a*, 0,0,0,0,0,0,0,0,0)	(0,0,0)	(0,*b*,*c*)	($\bar{2}$,2,0)(0,0,2)(1,1,0)	($\frac{1}{2}$,0,$\frac{1}{2}$)
2 $P\bar{1}$	(0,*a*,−*a*, 0,0,0,0,0,0,0,0,0)	(0,0,0)	(*b*,*c*,*d*)	(0,0,2)(1,1,0)($\bar{2}$,2,0)	($\frac{1}{2}$,0,$\frac{1}{2}$)
14 $P2_1/c$	(0,*a*,−*a*, 0,0,0,0,0,0,0,0,0)	(0,*b*,0)	(*c*,0,0)	($\bar{2}$,2,0)(0,0,2)(2,2,0)	(0,$\frac{3}{2}$,$\frac{1}{2}$)
26 $Pmc2_1$	(0,*a*,−*a*, 0,0,0,0,0,0,0,0,0)	(*b*,0,0)	(0,*c*,*c*)	(0,0,2)(2,$\bar{2}$,0)(1,1,0)	($\frac{3}{4}$,$\frac{1}{4}$,$\frac{1}{2}$)
31 $Pmn2_1$	(0,*a*,−*a*, 0,0,0,0,0,0,0,0,0)	(*b*,0,0)	(0,*c*,−*c*)	(0,0,2)(2,$\bar{2}$,0)(1,1,0)	($\frac{3}{4}$,$\frac{1}{4}$,$\frac{1}{2}$)
6 *Pm*	(0,*a*,−*b*, 0,0,0,0,0,0,0,0,0)	(*c*,0,0)	(0,*d*,*e*)	($\bar{2}$,2,0),(0,0,2),(1,1,0)	(0,0,$\frac{1}{2}$)

Table 6). There is no charge ordering in this prototypical Zener polaron structure, since the structure provides only a single Mn site.

Once again we make use of *ISOTROPY* to examine the effects on each of these structures [arising from $\Sigma_2(P1)$, $\Sigma_1(P2)$ and $\Sigma_2(P2)$] of the octahedral tilting associated with irreps M_3^+ and R_4^+. The results from these analyses are given in Tables 4–6. These were obtained from the *ISOTROPY* output, first by selecting those structures with order parameter *P*1 or *P*2 for irrep Σ_1 or Σ_2 as appropriate, then removing those showing non-zero M_3^+ and R_4^+ tilts around the same axis (*i.e.* corresponding components of the two relevant order parameters both non-zero). Finally we added to Tables 5 and 6 structures with M_3^+ tilting, but with order-parameter direction for Σ_1 or Σ_2 permitted to vary from *P*2 (the two components were no longer constrained to be numerically equal), to provide for M_3^+ tilt systems that otherwise would be inaccessible. The results are also illustrated in Figs. 6–8, which show the space groups for the structures obtained, along with the schematics of the group–subgroup relationships. Should the orbital ordering depicted in Fig. 5(*b*) be incorporated into the bistripe model, then the starting structure is the one with space-group symmetry $Pmc2_1$ order parameters (*a*,0,0)(0,0,0) and in Fig. 7 only the three structures descended from this starting structure need be considered.

A number of remarks are in order. First we note from the tables that tilt order parameters (*b*,0,0) and (0,*b*,0) lead to different structures, as do tilt order parameters (0,*b*,*b*) and (0,*b*,−*b*). The former difference is explained since we have set all our long-range patterns in the (001) plane, so octahedral tilting around axes perpendicular to this plane is expected to give structures different from those obtained when tilting is around axes lying in the plane. As to the latter differences, (0,*b*,*b*) corresponds to tilting around the shorter (length $2^{1/2}a_p$) and (0,*b*,−*b*) to tilting around the longer $(2(2)^{1/2}a_p)$ of the axes in the (001) plane. We mentioned earlier that the Zener polaron model, in space group *Pbam*, which we take to be its 'pure' form, does not permit charge ordering on the Mn sites. It is found, however, that for the structures in Table 6 in $Pmc2_1$, $Pmn2_1$, *C*2/*m*, *Cm*, *P*2/*m*, $P\bar{1}$, and for the last of the $P2_1/c$ structures in that table, the order parameters (listed using COPL) include $\Sigma_1(P2)$, corresponding to the bistripe pattern of charge ordering. It is therefore unsurprising that the identical structures appear in Table 5. Thus, for the particular tilt systems presented by these structures, the Zener polaron model cannot be distinguished from the bistripe model by means of space-group symmetry alone. This can be seen to justify, within the applicable tilt system, the identification of the Zener polaron model with the scheme of Mn^{3+} orbital ordering, which might be associated with this bistripe charge ordering (Subías *et al.*, 2006) but would by virtue of associated atomic displacements lower the space-group symmetry to $Pmc2_1$, is incorporated into Fig. 5(*b*).

The salient feature of the Zener polaron model is the formation of Mn dimers. This means we must examine the Mn displacements for patterns which will bring Mn atoms together in pairs. Irrep Σ_2 (direction *P*2) leads to displacements in directions [1$\bar{1}$0] and [$\bar{1}$10], the sense of the displacement being the same in two successive (110) planes then reversed in the next two planes. As can be seen in Fig. 5(*c*), these displacements do lead to Mn ions forming pairs, the dimers being indicated on the figure. The arrangement corresponds with schematic illustrations of the Zener polaron model that have appeared elsewhere (Efremov *et al.*, 2004; Coey, 2004; Subías *et al.*, 2006). The structure arising from $\Sigma_2(P2)$ has space-group symmetry *Pbam* on a $2(2)^{1/2}a_p \times 2^{1/2}a_p \times a_p$ cell (see

bistripe model (Goff & Attfield, 2004). On the possibility of ferroelectricity (*cf.* Efremov *et al.*, 2004), we see that all the structures in Table 4, based on the $\Sigma_2(P1)$ (checkerboard) distortion, are centrosymmetric. On the other hand, as can be seen in Tables 5 and 6, the combination of a component of M_3^+ tilting with either $\Sigma_1(P2)$ (bistripe) or $\Sigma_2(P2)$ (Zener polaron) distortion has a propensity to give structures with non-centrosymmetric and indeed polar space-group symmetries, in which ferroelectricity might well be expected.

There remains the question as to what extent the different models proposed might be distinguished by different space-group symmetries. For compounds in *Imma* at room temperature that maintain the *Imma* tilt system [order parameters for M_3^+ and R_4^+ being (0,0,0) and $(0,b,-b)$ respectively, and Glazer symbol $a^-a^-c^0$] in the low-temperature charge and/or orbitally ordered variant, the checkerboard, bistripe and Zener polaron models give structures in the space groups *Pmmm*, *Pmna* and *Pnnm*. $Nd_{1/2}Sr_{1/2}MnO_3$ is thought to behave in this way (Woodward *et al.*, 1999), but the space-group symmetry of the low-temperature variant does not seem to have been determined. For compounds such as $La_{1/2}Ca_{1/2}MnO_3$ and $Pr_{1/2}Ca_{1/2}MnO_3$ that have structures in *Pnma* [order parameters for M_3^+ and R_4^+ being $(b,0,0)$ and $(0,c,-c)$ respectively,[8] $a^-a^-c^+$] at room temperature, it should be possible to distinguish the checkerboard model for charge and orbital ordering, giving a structure in $P2_1/m$, from the other two models, which give the space-group symmetry of the low-temperature variant as $Pmn2_1$. Both these space groups have been reported (Radaelli *et al.*, 1997; Daoud-Aladine *et al.*, 2002; Goff & Attfield, 2004). However, we are somewhat persuaded by the use of electron diffraction to determine reflection conditions (Wu *et al.*, 2007), and the conclusion that the space-group symmetry of the ordered phase of $Pr_{1/2}Ca_{1/2}MnO_3$ is $Pmn2_1$. This agrees with the expectation for either the bistripe or Zener polaron model.

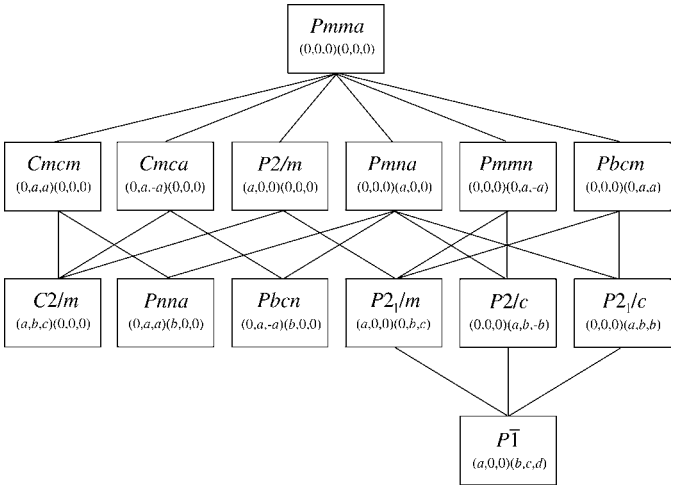

Figure 6
A schematic diagram showing the group–subgroup relationships among the structures formed in half-doped manganites with 'striped' or 'checkerboard-type' charge and/or orbital ordering on manganese ions. The tilt systems here are specified not by the Glazer symbols but rather by the order parameters for irreps M_3^+ and R_4^+. The lines connecting structures indicate group–subgroup relationships and all the corresponding transitions are, in Landau theory, allowed to be continuous. Details of the structures are recorded in Table 4.

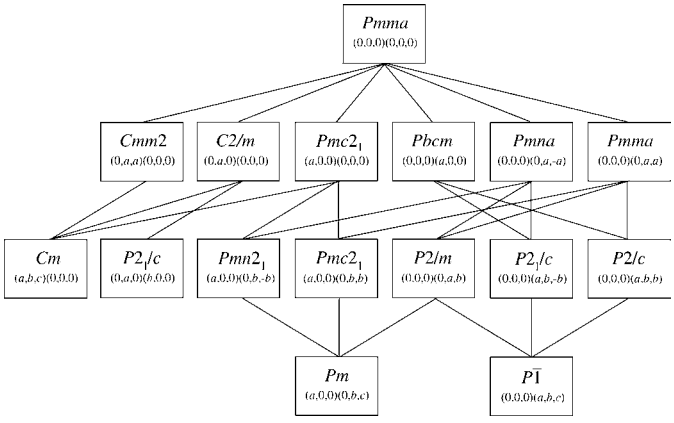

Figure 7
A schematic diagram showing the group–subgroup relationships among the structures formed in half-doped manganites with 'bistriped' ordering of manganese ions. The presentation is as in Fig. 6 and details of the structures are recorded in Table 5. For the orbital ordering depicted in Fig. 6(*b*), and the atomic displacements expected to result from that, the starting structure is that in $Pmc2_1$ order parameters $(a,0,0)(0,0,0)$, and only the structures descended from this need to be considered.

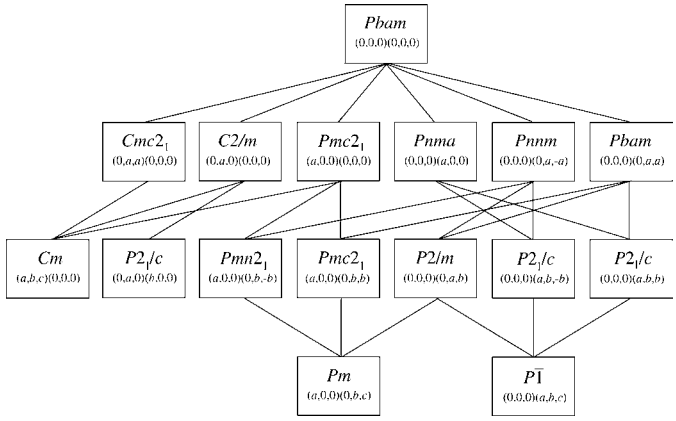

Figure 8
A schematic diagram showing the group–subgroup relationships among the structures formed in half-doped manganites according to the 'Zener polaron', 'bond-centred' or dimer model of ordering. The presentation is as in Fig. 6 and details of the structures are recorded in Table 6.

6. Summary and conclusions

The structures obtained by combining octahedral tilting with ordered arrangements of JT and non-JT *B*-site cations in $A_2BB'X_6$ perovskites have been listed, and the group–subgroup relationships shown. Results are given for both rock-salt and checkerboard ordering of the *B* and *B*′ cations. To ensure that the JT distortions are properly attached to the JT

[8] The order parameter including the minus sign is preferred because it selects the same structures, *e.g.* that in $Pmn2_1$, as are found from the *Pnma* perovskite subject to X point distortions. This choice corresponds to tilting around the longest axis.

Table 6
Space groups, order-parameter components, and unit-cell relationships for the Zener polaron model for ordering in manganites, associated with the irrep Σ_2 ($\boldsymbol{k} = \xi,\xi,0$, $\xi = 1/4$).

The presentation of results is as in Table 4.

Space group	Σ_2	M_3^+	R_4^+	Lattice vectors	Origin
55 *Pbam*	(0,*a*,−*a*, 0,0,0,0,0,0,0,0)	(0,0,0)	(0,0,0)	(2,$\bar{2}$,0)(1,1,0)(0,0,1)	($\frac{1}{2}$,0,0)
26 *Pmc*2_1	(0,*a*,−*a*, 0,0,0,0,0,0,0,0)	(*b*,0,0)	(0,0,0)	(0,0,1)(2,$\bar{2}$,0)(1,1,0)	($\frac{1}{4}$,$\frac{3}{4}$,0)
12 *C*2/*m*	(0,*a*,−*a*, 0,0,0,0,0,0,0,0)	(0,*b*,0)	(0,0,0)	(2,2,0)(0,0,2)(2,$\bar{2}$,0)	(0,$\frac{3}{2}$,$\frac{1}{2}$)
36 *Cmc*2_1	(0,*a*,−*b*, 0,0,0,0,0,0,0,0)	(0,*c*,*c*)	(0,0,0)	(0,0,2)(2,2,0)($\bar{2}$,2,0)	($\frac{1}{2}$,$\frac{1}{2}$,$\frac{1}{2}$)
8 *Cm*	(0,*a*,−*b*, 0,0,0,0,0,0,0,0)	(*c*,*d*,*e*)	(0,0,0)	(2,2,0)(0,0,2)(2,$\bar{2}$,0)	($\frac{1}{2}$,$\frac{1}{2}$,$\frac{1}{2}$)
62 *Pnma*	(0,*a*,−*a*, 0,0,0,0,0,0,0,0)	(0,0,0)	(*b*,0,0)	(1,1,0)(0,0,2)(2,$\bar{2}$,0)	($\frac{1}{2}$,0,$\frac{1}{2}$)
55 *Pbam*	(0,*a*,−*a*, 0,0,0,0,0,0,0,0)	(0,0,0)	(0,*b*,*b*)	(2,$\bar{2}$,0)(1,1,0)(0,0,2)	($\frac{1}{2}$,0,$\frac{1}{2}$)
58 *Pnnm*	(0,*a*,−*a*, 0,0,0,0,0,0,0,0)	(0,0,0)	(0,*b*,−*b*)	(2,$\bar{2}$,0)(1,1,0)(0,0,2)	($\frac{1}{2}$,0,$\frac{1}{2}$)
14 *P*2_1/*c*	(0,*a*,−*a*, 0,0,0,0,0,0,0,0)	(0,0,0)	(*b*,*c*,*c*)	(0,0,2)(2,$\bar{2}$,0)(1,1,0)	($\frac{1}{2}$,0,$\frac{1}{2}$)
14 *P*2_1/*c*	(0,*a*,−*a*, 0,0,0,0,0,0,0,0)	(0,0,0)	(*b*,*c*,−*c*)	(0,0,2)(1,1,0)($\bar{2}$,2,$\bar{2}$)	($\frac{1}{2}$,0,$\frac{1}{2}$)
10 *P*2/*m*	(0,*a*,−*a*, 0,0,0,0,0,0,0,0)	(0,0,0)	(0,*b*,*c*)	($\bar{2}$,2,0)(0,0,2)(1,1,0)	($\frac{1}{2}$,0,$\frac{1}{2}$)
2 $P\bar{1}$	(0,*a*,−*a*, 0,0,0,0,0,0,0,0)	(0,0,0)	(*b*,*c*,*d*)	(0,0,2)(1,1,0)($\bar{2}$,2,0)	($\frac{1}{2}$,0,$\frac{1}{2}$)
14 *P*2_1/*c*	(0,*a*,−*a*, 0,0,0,0,0,0,0,0)	(0,*b*,0)	(*c*,0,0)	($\bar{2}$,2,0)(0,0,2)(2,2,0)	(0,$\frac{3}{2}$,$\frac{1}{2}$)
26 *Pmc*2_1	(0,*a*,−*a*, 0,0,0,0,0,0,0,0)	(*b*,0,0)	(0,*c*,*c*)	(0,0,2)(2,$\bar{2}$,0)(1,1,0)	($\frac{1}{4}$,$\frac{1}{4}$,$\frac{1}{2}$)
31 *Pmn*2_1	(0,*a*,−*a*, 0,0,0,0,0,0,0,0)	(*b*,0,0)	(0,*c*,−*c*)	(0,0,2)(2,$\bar{2}$,0)(1,1,0)	($\frac{1}{4}$,$\frac{1}{4}$,$\frac{1}{2}$)
6 *Pm*	(0,*a*,−*b*, 0,0,0,0,0,0,0,0)	(*c*,0,0)	(0,*d*,*e*)	($\bar{2}$,2,0),(0,0,2),(1,1,0)	(0,0,$\frac{1}{2}$)

active ions, the irreps associated with the distortions and the irreps describing the cation ordering must belong to the same point in the Brillouin zone. In the case of rock-salt ordering, certain of the listed structures have been reported in the literature. The authors are not aware of any structures corresponding to the simple checkerboard ordering, for reasons which are not yet understood.

The more complex and longer-range patterns that occur in certain half-doped manganites at lower temperatures have also been examined. Three models for this ordering have been considered. The first, described as checkerboard or stripe charge ordering, is found from the perspective of the cubic parent in $Pm\bar{3}m$ to be primarily an orbital ordering with concomitant JT distortions, the checkerboard pattern of charge disproportionation arising as a secondary effect. Experimental evidence on the degree of charge separation poses conceptual problems for this model, at least in its original form. The second is a bistripe pattern of charge ordering. The third, known as the Zener polaron model, involves the formation of Mn dimers, and in its prototypical form does not permit charge ordering. On combining octahedral tilting with these arrangements, we find that all structures obtained from the checkerboard pattern are centrosymmetric. On the other hand, combining the tilting associated with irrep M_3^+ with either bistripe charge ordering or the Zener polaron arrangement gives a number of structures in non-centrosymmetric and polar space groups; thus ferroelectricity is to be expected. Various combinations of tilting with the Zener polaron starting structure do support a bistripe pattern of charge disproportionation, and for each of these tilt systems both bistripe and Zener polaron models yield the same structure. It may be possible nevertheless to distinguish the three models for structures that have and maintain the tilt system ($a^-a^-c^0$) of the simple *Imma* perovskite, and for those with the *Pnma* tilt system ($a^-a^-c^+$) it should be possible to distinguish the checkerboard model from the other two. A recent electron diffraction determination of the space group of $Pr_{1/2}Ca_{1/2}MnO_3$ (tilt system $a^-a^-c^+$) as *Pmn*2_1 (Wu *et al.*, 2007) favours the bistripe or Zener polaron model for this compound.

The authors thank Professor Harold Stokes, Brigham Young University, for his comment on a draft of this manuscript. They also acknowledge the support of the Leverhulme Trust, in the form of a Visiting Professorship for CJH. The work is supported by the Australian Research Council, grant DP0877695.

References

Argyriou, D. N., Hinks, D. G., Mitchell, J. F., Potter, C. D., Scultz, A. J., Young, D. M., Jorgensen, J. D. & Bader, S. D. (1996). *J. Solid State Chem.* **124**, 381–384.

Blasco, J., García, J., De Teresa, J. M., Ibarra, M. R., Perez, J., Algarabel, P. A., Marquina, C. & Ritter, C. (1997). *J. Phys. Condens. Matter*, **9** 10321.

Caignaert, V., Millange, F., Hervieu, M., Suard, E. & Raveau, B. (1996). *Solid State Commun.* **99**, 173–177.

Campbell, B. J., Stokes, H. T., Tanner, D. E. & Hatch, D. M. (2006). *J. Appl. Cryst.* **39**, 607–614.

Carpenter, M. A. & Howard, C. J. (2009). *Acta Cryst.* B**65**, 134–146.

Chahara, K.-I., Ohno, T., Kasai, M. & Kozono, Y. (1993). *Appl. Phys. Lett.* **63**, 1990–1992.

Chatterji, T. (2004). Editor. *Colossal Magnetoresistive Manganites.* Dordrecht, The Netherlands: Kluwer Academic Publishers.

Cheah, M., Saines, P. J. & Kennedy, B. J. (2006). *J. Solid State Chem.* **179**, 1775–1781.

Cheong, S.-W. & Mostovoy, M. (2007). *Nature Mater.* **6**, 13–20.

Coey, M. (2004). *Nature*, **430**, 155–157.

CrystalMaker Software Ltd (2009). *CrystalMaker*. CrystalMaker Software Ltd, Oxford, UK.

Damay, F., Martin, C., Hervieu, M., Maignan, A., Raveau, B., André, G. & Bourée, F. (1998). *J. Magn. Magn. Mater.* **184**, 71–82.

Daoud-Aladine, A., Rodríguez-Carvajal, J., Pinsard-Gaudart, L., Fernández-Díaz, M. T. & Revcolevschi, A. (2002). *Phys. Rev. Lett.* **89**, 097205.

Eerenstein, W., Mathur, N. D. & Scott, J. D. (2006). *Nature*, **442**, 759–765.

Efremov, D. V., van den Brink, J. & Khomskii, D. I. (2004). *Nature Mater.* **3**, 853–856.

Glazer, A. M. (1972). *Acta Cryst.* B**28**, 3384–3392.

Gateshki, M. & Igartua, J. M. (2003). *J. Phys. Condens. Matter*, **15**, 6749–6757.

Gateshki, M., Igartua, J. M. & Hernández-Bocanegra, E. (2003). *J. Phys. Condens. Matter*, **15**, 6199–6217.

Goff, R. J. & Attfield, J. P. (2004). *Phys. Rev. B*, **70**, 140404(R).

Goodenough, J. B. (1955). *Phys. Rev.* **100**, 564–573.

Goodenough, J. B. (1998). *Ann. Rev. Mater. Sci.* **28**, 1–27.

Goodenough, J. B. (2004). *Rep. Prog. Phys.* **67**, 1915–1993.

Helmolt, R. von, Wecker, J., Holzapfel, B., Schultz, L. & Samwer, K. (1993). *Phys. Rev. Lett.* **71**, 2331–2333.

Hervieu, M., Maignan, A., Martin, C., Nguyen, N. & Raveau, B. (2001). *Chem. Mater.* **13**, 1356–1363.

Howard, C. J., Kennedy, B. J. & Woodward, P. M. (2003). *Acta Cryst.* B**59**, 463–471.

Howard, C. J. & Stokes, H. T. (1998). *Acta Cryst.* B**54**, 782–789.

Howard, C. J. & Stokes, H. T. (2005). *Acta Cryst.* A**61**, 93–111.

Ivanov, S. A., Nordblad, P., Tellgren, R. & Hewat, A. W. (2009). *Mater. Res. Bull.* **44**, 822–830.
Jin, S., McCormack, M., Tiefel, T. H. & Ramesh, R. (1994). *J. Appl. Phys.* **76**, 6929–6933.
Jirák, Z., Damay, F., Hervieu, M., Martin, C., Raveau, B., André, G. & Bourée, F. (2000). *Phys. Rev. B*, **61**, 1181–1188.
Jirák, Z., Krupička, S., Šimša, Z., Dlouhá, M. & Vratislav, S. (1985). *J. Magn. Magn. Mater.* **53**, 153–166.
Ju, H. L., Nam, Y. S., Lee, J. E. & Shin, H. S. (2000). *J. Magn. Magn. Mater.* **219**, 1–8.
Kisi, E. H. & Howard, C. J. (2008). *Applications of Neutron Powder Diffraction.* Oxford University Press.
Loudon, J. C., Cox, S., Williams, A. J., Attfield, J. P., Littlewood, P. B., Midgley, P. A. & Mathur, N. D. (2005). *Phys. Rev. Lett.* **94**, 097202.
Lufaso, M. W., Gemmill, W. R., Mugavero, S. J., Kim, S.-J., Lee, Y., Vogt, T. & zur Loye, H.-C. (2008). *J. Solid State Chem.* **181**, 623–627.
Lufaso, M. W. & Woodward, P. M. (2004). *Acta Cryst.* B**60**, 10–20.
Mclaughlin, A. C. (2008). *Phys. Rev. B*, **78**, 132404.
Millis, A. J. (1998). *Nature*, **392**, 147–150.
Radaelli, P. G., Cox, D. E., Marezio, M. & Cheong, S.-W. (1997). *Phys. Rev. B*, **55**, 3015–3023.
Radaelli, P. G., Cox, D. E., Marezio, M., Cheong, S.-W., Schiffer, P. E. & Ramirez, A. P. (1995). *Phys. Rev. Lett.*, **75**, 4488–4491.
Rodríguez-Carvajal, J., Hennion, M., Moussa, F., Moudden, A. H., Pinsard, L. & Revcolevschi, A. (1998). *Phys. Rev. B*, **57**, R3189–R3192.
Shimomura, S., Tajima, K., Wakabayashi, N., Kobayashi, S., Kuwahara, H. & Tokura, Y. (1999). *J. Phys. Soc. Jpn*, **68**, 1943–1947.
Stokes, H. T. & Hatch, D. M. (2001). *COPL*, http://stokes.byu.edu/isotropy.html.
Stokes, H. T., Hatch, D. M. & Campbell, B. J. (2007). *ISOTROPY*, http://stokes.byu.edu/isotropy.html.
Subías, G., García, J., Beran, P., Nevřiva, M., Sánchez, M. C. & García-Muñoz, J. L. (2006). *Phys. Rev. B*, **73**, 205107**.**
Sundaresan, A., Paulose, P. L., Mallik, R. & Sampathjumaran, E. V. (1998). *Phys. Rev. B*, **57**, 2690–2693.
Wollan, E. O. & Koehler, W. C. (1955). *Phys. Rev.* **100**, 545–563.
Woodward, P. M., Cox, D. E., Vogt, T., Rao, C. N. R. & Cheetham, A. K. (1999). *Chem. Mater.* **11**, 3528–3538.
Wu, L., Klie, R. F., Zhu, Y. & Jooss, Ch. (2007). *Phys. Rev. B*, **76**, 174210.